

Confinement and manipulation of electron plasmas in a multicell trap

Cite as: Phys. Plasmas **26**, 013513 (2019); <https://doi.org/10.1063/1.5078649>

Submitted: 26 October 2018 . Accepted: 07 December 2018 . Published Online: 24 January 2019

N. C. Hurst , J. R. Danielson, C. J. Baker, and C. M. Surko

COLLECTIONS

 This paper was selected as an Editor's Pick



View Online



Export Citation



CrossMark



Confinement and manipulation of electron plasmas in a multicell trap

Cite as: Phys. Plasmas **26**, 013513 (2019); doi: [10.1063/1.5078649](https://doi.org/10.1063/1.5078649)

Submitted: 26 October 2018 · Accepted: 07 December 2018 · Published Online: 24 January 2019



View Online



Export Citation



CrossMark

N. C. Hurst,^{a)}  J. R. Danielson,^{b)} C. J. Baker,^{c)} and C. M. Surko

AFFILIATIONS

Department of Physics, University of California San Diego, 9500 Gilman Drive, La Jolla, California 92093, USA

^{a)} nhurst@physics.ucsd.edu

^{b)} jrdanielson@ucsd.edu

^{c)} Present address: Department of Physics, College of Science, Swansea University, Swansea, United Kingdom.

ABSTRACT

Plasma dynamics and transport are studied experimentally in a multicell Penning-Malmberg trap. The goal is to develop methods for accumulation and long-term confinement of larger numbers of charged particles (e.g., positrons) than is presently possible. In this scheme, the particles constitute non-neutral plasmas which are confined separately in a parallel array of storage cells. Experiments are presented in which pure electron plasmas are transferred from a large-diameter “master cell” trapping region into four smaller, parallel “storage cells,” three of which are offset from the magnetic symmetry axis. The physics of the transfer process, as well as the confinement properties of plasmas in the storage cells, is discussed. We show that plasmas can be transferred into the storage cells and held there for up to a day or more using the rotating wall technique, provided that the plasma radius is sufficiently small compared to that of the cell wall. Experiments regarding the confinement of plasmas with kilovolt space charge are discussed. Recommendations are provided for future efforts with high-capacity multicell traps.

Published under license by AIP Publishing. <https://doi.org/10.1063/1.5078649>

I. INTRODUCTION

Non-neutral, single-component plasmas have been studied extensively in the laboratory, motivated by a variety of interesting physical properties and several important applications.^{1–3} These plasmas are typically confined in a Penning-Malmberg (PM) trap,² a device where radial confinement is achieved using a strong, axial, applied magnetic field, and axial confinement is achieved by biasing a set of cylindrical electrodes to create an electrostatic potential well. Excellent confinement properties are routinely observed in PM traps since the canonical angular momentum of the plasma is constrained due to the cylindrical symmetry.⁴ As a result, PM devices have become a standard for storing and manipulating large numbers of antiparticles (e.g., positrons or antiprotons).^{3,5} In this application, the trapped antiparticles typically constitute a cylindrical plasma which rotates about its axis due to the $\mathbf{E} \times \mathbf{B}$ drift. By creating ultra-high vacuum (UHV) conditions and countering outward radial particle transport with the so-called “rotating wall” (RW) technique,^{6,7} the antiparticles can be kept from annihilating and can be stored for days or more.³

This technology has had a substantial impact on the field of antimatter science. For example, PM traps have been used in the

first laboratory realization of stable, trapped antihydrogen.⁸ Cryogenic positron plasmas have been used recently to generate positron beams with narrow energy spreads,⁹ with applications in antimatter chemistry and atomic physics. Some applications require large bursts of positrons, which can be accomplished in the laboratory using a PM trap; they include efforts to create a Bose-condensate of positronium molecules¹⁰ and efforts to create and study an electron-positron plasma.¹¹

However, there are practical limitations to the number of charged particles which can be stored in a PM trap. The plasma generates a space-charge potential which is given approximately by

$$|\phi(r=0)| = \frac{eN}{4\pi\epsilon_0 L} \left[1 + 2 \ln \left(\frac{r_w}{r_p} \right) \right], \quad (1)$$

(SI units) on the cylindrical axis, where ϵ_0 is the permittivity of free space, e is the electron charge, r_p and r_w are the radii of the plasma and of the trap electrodes, N is the number of particles, and L is the axial length of the plasma. Thus, for given trap dimensions, N is constrained by the confinement voltage V_c applied to the endcap electrodes. Voltages of $V_c \sim 1\text{ kV}$ have

been implemented successfully,^{12,13} but higher voltages can introduce plasma heating and other deleterious effects.

To circumvent these problems, a multicell trap design was proposed,¹⁴ where many separate plasmas can be confined simultaneously in an array of parallel PM traps called “storage cells.” In this way, the individual plasmas are electrically shielded from one another, and so, N can be increased without increasing ϕ . Experiments were conducted with electron plasmas in a single PM trap to analyze the feasibility of the multicell concept.^{12,15} Here, $N \sim 10^{10}$ was achieved using $V_c = 1$ kV, and it was estimated that $N \sim 10^{12}$ could be possible using a multicell device with 21 cells.

The operation of a multicell trap is expected to involve a considerable number of procedures which have not been previously studied in detail. Described here are tests of a prototype multicell device which includes a large-diameter “master cell” and four small diameter “storage cells,” three of which are offset from the magnetic symmetry axis. The principal goals were to develop a robust mechanical structure for the multicell trap electrodes; demonstrate the ability to move plasmas off of the magnetic axis and deposit them in off-axis cells; optimize plasma confinement in off-axis cells with space charge potential ranging up to a kilovolt; establish that plasmas can be held for hours or more in off-axis cells using the RW technique; operate multiple cells simultaneously; and keep particle losses at a minimum. One of the primary challenges is to counter outward radial expansion of the plasma. This can be accomplished in principle using the RW technique, strong cooling *via* cyclotron radiation in a high magnetic field (i.e., several tesla),¹⁶ and careful engineering of the electrodes to avoid transport due to mechanical or electrical asymmetries.¹⁷

We report here that plasmas have been transferred successfully into off-axis cells of the prototype multicell trap, where they were confined using the RW technique for more than a day in certain cases. However, progress was limited due to poor confinement in the storage cells, likely due to asymmetry-induced expansion. Accordingly, the goals of high space charge and multiple cell operation are yet to be realized.

The remainder of this paper is organized as follows: Details of the experimental apparatus are given in Sec. II, radial displacement of plasmas in the master cell is discussed in Sec. III, the physics of the transfer process is discussed in Sec. IV (between coaxial cells) and Sec. V (non-coaxial), and storage cell confinement studies are given in Sec. VI. Related experiments with kilovolt confinement potentials are given in Sec. VII. Finally, concluding remarks are made in Sec. VIII, including recommendations for future efforts with multicell trap devices.

II. EXPERIMENTAL SETUP

The prototype multicell trap apparatus^{12,18} is shown in Fig. 1, including a computer model of the electrode structure and a schematic diagram of the storage cell arrangement. Cell A shares its symmetry axis with the master cell (M), while cells B, C, and D are offset. The electrodes are constructed from gold-plated aluminum. They are electrically isolated by Macor ceramic spacers. The structure is held together in compression by a set of threaded titanium rods.

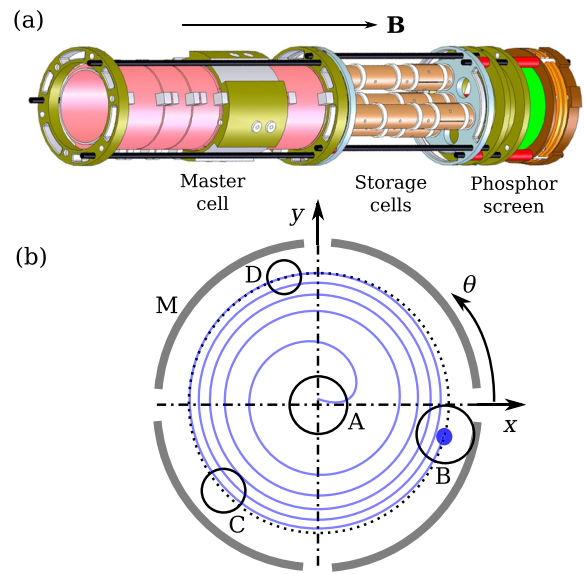


FIG. 1. Geometry of the multicell trap apparatus, including (a) a solid computer model of the electrodes and (b) a schematic of the master (M) and storage cell (A–D) layout in the plane perpendicular to the magnetic field. Also shown in panel (b) is a typical spiral trajectory of a plasma when driven toward an off-axis cell (blue line, see Sec. III).

Typically, plasmas are generated in the master cell, then transferred into one of the four storage cells, and finally diagnosed using a phosphor screen which is mounted to the end of the structure and biased to +5 kV. The entire structure is placed inside a vacuum chamber which is evacuated to a pressure of $\sim 10^{-9}$ torr. It is immersed in an axial magnetic field of $B = 4.8$ T which is approximately uniform over the region of the electrodes, with variations $\delta B/B \approx 0.01$. The dimensions and locations of the master cell (M) and storage cells (A–D) are given in Table I.

The storage cells were built with different radii r_w in order to determine experimentally the minimum acceptable dimensions. In principle, the number of cells that can be arranged in a specific vacuum and magnet system scales as r_w^{-2} , and so, smaller storage cells are beneficial as long as the radial confinement is sufficiently good.

TABLE I. Geometry of the master cell (M) and storage cells (A–D) in the prototype multicell trap apparatus, including the wall radius r_w , axial trapping length L_t , and radial and azimuthal location (r, θ) .

Cell	r_w [mm]	L_t [mm]	(r, θ) [mm, °]
M	38	155	(0, –)
A	8	150	(0, –)
B	8	150	(30, 345)
C	6	150	(30, 225)
D	4	150	(30, 105)

The arrangement of the electrodes and the experimental procedure are shown schematically in Fig. 2. The master cell consists of five electrodes M1-M5. Electrode M4 is partitioned into four equal azimuthal segments, which are used to apply a rotating transverse electric field for RW compression of the plasma,⁶ as well as to launch and detect asymmetric electrical signals. The storage cells each consist of six electrodes, S1-S6 (where the label “S” refers generically to a storage cell). Electrodes A5, B4, C4, and D4 are segmented just as cell M4 in order to apply RW compression in each cell. The distance between the confining electrodes is called the “trap length” L_t ; the plasma length L can be calculated from the trap dimensions and the plasma properties.¹⁹ These lengths can be varied by biasing different electrodes,¹⁸ however, for most of the data presented here, the longest available trapping region was used (e.g., plasmas are trapped between M1 and M5 or between S1 and S6). A flat electrode called the front plate (FP) provides electrical shielding between the master and storage cells, in order to minimize asymmetry-induced transport in the storage cells (i.e., due to the master cell electrodes). It has circular holes matching the radii of the storage cells, and it is electrically connected to the electrodes S1 on each of the storage cells.

Experiments are conducted in the following manner: First, plasmas are generated in the master cell using a heated-cathode electron source located in the fringing region of the magnetic field nearest the master cell. During plasma generation, electrode M5 is biased to the confinement voltage V_c (typically -100 V), M1 is biased to voltage V_1 where $0 < |V_1| < |V_c|$, and the electron source is biased to voltage V_e , where $|V_1| < |V_e| < |V_c|$. In this way, electrons can become trapped by scattering energy into the perpendicular direction while transiting the master cell electrodes.²⁰ Once trapped, the plasma cools *via* cyclotron

radiation in the strong magnetic field to a temperature $T \sim 0.1$ eV, on a timescale of $\tau_c \propto B^{-2} \approx 0.2$ s.¹⁶ Most of the plasmas discussed here have particle number $N \approx 10^8$ – 10^9 , radius $r_p \approx 0.5$ – 3 mm, peak density $n \approx 10^5$ – 10^7 mm⁻³, space charge potential $\phi \approx 10$ – 40 V (master cell) or 5 – 20 V (storage cells), and length $L \approx 100$ – 140 mm (master cell) or 130 – 140 mm (storage cells).

The RW technique is used in the master cell to reduce the plasma radius, so as to facilitate transfer into the storage cells. Since the symmetry axis of cell A coincides with that of the master cell, plasma transfers into cell A are accomplished by holding electrodes M1 and A6 at voltage V_c and grounding M5 and A1 for some time such that plasma streams along the magnetic field into the storage cell (in some cases, electrodes A2–A5 are also biased, as discussed in Sec. IV). Alternatively, plasmas can be generated directly in cell A using the technique described above.

In order to transfer the plasma into the off-axis cells (B, C, and D), it must be displaced across the magnetic field. This is accomplished using autoresonant control of the $m = 1$ diocotron mode,^{15,18,21} which is a type of $\mathbf{E} \times \mathbf{B}$ drift wave where m is an azimuthal wavenumber. The plasma is moved radially outward in a spiral pattern using a chirped drive signal applied to one segment of electrode M4. The drive signal is turned off when the radial location of the plasma coincides with the storage cells, at which point the transfer procedure (described above for the coaxial cell) is initiated. After the transfer, the plasma in the storage cell is isolated by biasing electrode S1 to voltage V_c , and the RW technique is implemented in the storage cell to counter expansion.

The areal (i.e., 2D) density profile of the plasma is then diagnosed destructively using the phosphor screen and a CCD camera. Here, the confinement electrode nearest the screen (i.e., M5 or S6) is grounded, such that the plasma streams along the magnetic field onto the phosphor screen (master cell plasmas can only be imaged when passing through the storage cells). The resulting fluorescent light is recorded by a CCD camera located in the fringing magnetic field on the side of the screen opposite the electron source. The resolution of the CCD diagnostic is about $55 \mu\text{m}/\text{pixel}$, and the signal-to-noise ratio is of order 10^2 . Additionally, plasma waves (e.g., diocotron modes) can be diagnosed *in situ* by receiving electrical signals on the segmented electrodes.

III. AUTORESONANT DIOCOTRON DRIVE

The dynamics of plasmas in the master cell during autoresonant control of the diocotron mode have already been discussed in detail.¹⁸ Here, we provide a brief summary of those results in the broader context of the multicell trap research.

It was shown previously that plasmas in a standard PM trap could be positioned accurately in the plane perpendicular to B using autoresonant manipulation of the $m = 1$ diocotron mode.^{15,21} The diocotron mode is a type of $\mathbf{E} \times \mathbf{B}$ drift wave unique to non-neutral plasmas, where the wave propagates perpendicular to the magnetic field. For wavenumber $m = 1$, the diocotron mode corresponds to a circular drift orbit of the plasma about the symmetry axis due to image charges induced in the conducting boundary. If the plasma is long ($r_w/L \ll 1$) and

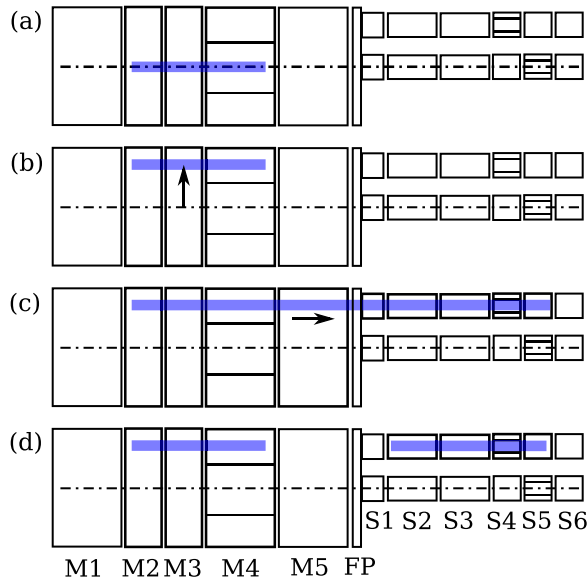


FIG. 2. Experimental procedure in the multicell trap: (a) plasmas are generated in the master cell; (b) they are displaced across the magnetic field; and they are (c) transferred into and (d) held in a storage cell.

the radius is small ($r_p/r_w \ll 1$), it can be treated as an infinite line charge, and the mode is described as a nonlinear oscillation with frequency

$$f_d = \frac{eN}{4\pi^2\epsilon_0BLr_w^2} \left[\frac{1}{1 - (d/r_w)^2} \right], \quad (2)$$

where d is the displacement of the plasma from the axis. In the storage cells, Eq. (2) is accurate to within a few percent. However, in the master cell, the ratio r_w/L is not small, and so, the mode frequency is changed due to 3D effects. Diocotron frequencies in the master cell have been predicted accurately using a numerical model¹⁹ based on prior analytical work.²²

The diocotron mode is driven by a transverse electric field, for example, by biasing one segment of the RW electrodes (M4 or S4). When the frequency of the drive signal is swept, the plasma oscillation can lock to the drive and adjust its mode amplitude accordingly; this phenomenon is known as autoresonance.²¹ In the master cell, a chirp waveform is applied to the drive electrode, which causes the plasma to move radially outward with a spiral trajectory [as depicted in Fig. 1(b)]. The drive signal is terminated when the plasma reaches the desired radius. Cell B corresponds to a displacement in the master cell $0.58 < d/r_w < 1$; cell C, $0.63 < d/r_w < 0.95$; and cell D, $0.68 < d/r_w < 0.89$. However, in order to successfully transfer plasmas, it is advantageous to position them close to the storage cell symmetry axis at $d/r_w = 0.79$ (see Sec. V for details).

Under some conditions, it was observed that autoresonant diocotron drive in the master cell caused the plasma to expand significantly at large mode amplitudes $d/r_w \geq 0.6$.¹⁸ Furthermore, the plasmas were completely destroyed upon reaching a critical mode amplitude of $d/r_w \approx 0.85$ – 0.9 . Alternatively, it was shown that when short master cell plasmas ($L \sim 40$ mm) were used, the transport was minimal and excitation to $d/r_w \approx 0.95$ was possible, although this reduces the particle storage capacity [cf. Eq. (1)].¹⁸ Confinement of plasma in the storage cells is difficult when r_p/r_w is sufficiently large (as discussed in Sec. VI), and so, expansion during autoresonant drive is undesirable. The expansion is thought to be due to a combination of asymmetry transport¹⁷ due to the driving field and rotational pumping²³ due to the curved confinement potentials, although spatial variations of B may also play a role.^{18,24} Plasma destruction may be associated with the driving field,²⁵ which is strong near the gaps between the segmented electrodes (although these events have not been diagnosed directly in the master cell). On the other hand, when the drive amplitude is too small, the diocotron mode either fluctuates significantly about the drive signal or completely fails to lock.¹⁸ With these considerations in mind, the autoresonant diocotron excitation should be accomplished quickly and with as weak a drive field as possible in order to reduce expansion and avoid plasma destruction.

IV. ON-AXIS TRANSFER

In this section, we discuss the process of transferring plasma from the master cell into the coaxial storage cell A. The more complicated situation of non-coaxial transfer is considered in Sec. V. These experiments begin with a plasma located on the symmetry axis of the master cell, with electrodes M1, M5,

A1, and A6 biased to voltage $V_c = -100$ V. At $t = 0$, electrodes M5 and A1 are ramped to ground within $1 \mu\text{s}$, allowing plasma to stream along the magnetic field into cell A. At some later time t , they are biased once again, isolating the plasma in cell A, which is then diagnosed and compared to the initial plasma. In these studies, the transferred plasma has the same radial distribution as the initial plasma, indicating that the dynamics are purely axial. The primary metric for these experiments is the “transfer efficiency,” defined as the ratio of the particle number transferred into the storage cell to that of the initial plasma N_s/N_0 . Although the free axial expansion of a pure electron plasma has been studied previously,²⁶ the situation is complicated here due to the difference in the wall radius of the two cells.

In general, the transfers can be characterized as “fast,” where the plasma quickly reaches a collisionless axial equilibrium on the order of a few bounce periods (i.e., $\tau_b = 2L/v_T \sim 1 \mu\text{s}$, where v_T is the thermal velocity) or “slow” where the plasma equilibrates axially due to collisions on timescales ≥ 1 ms. The fast transfer scheme exhibits a phenomenon called “anti-shielding,” where the plasma density is reduced in the vicinity of a positive potential (i.e., since particles are accelerated).²⁷ In this way, the storage cell density is reduced relative to the master cell due to a potential drop associated with the differing wall radii [cf. Eq. (1)]. Alternatively, during the slow transfer (collisional equilibrium), the plasma density adjusts to maintain constant potential between the two cells, resulting in a higher density in the storage cell. Transfers with unity efficiency can be achieved on slow timescales by creating a potential well in the storage cell (i.e., by biasing electrodes A2–A5 to $+100$ V). However, slow transfer into the off-axis cells is complicated due to diocotron mode dynamics (see Sec. V for details).²⁸ Note that unity efficiency can be achieved on intermediate timescales by adiabatically shortening the confinement region (i.e., by “squeezing” the plasma into the storage cell), although this may result in heating of the plasma.

Data are shown in Fig. 3 for the coaxial transfer efficiency as a function of the transfer time t for two different initial plasmas with $N_0 = 1.5 \times 10^8$ and 5.2×10^8 . For both plasmas, $r_p \approx 1$ – 1.2 mm.

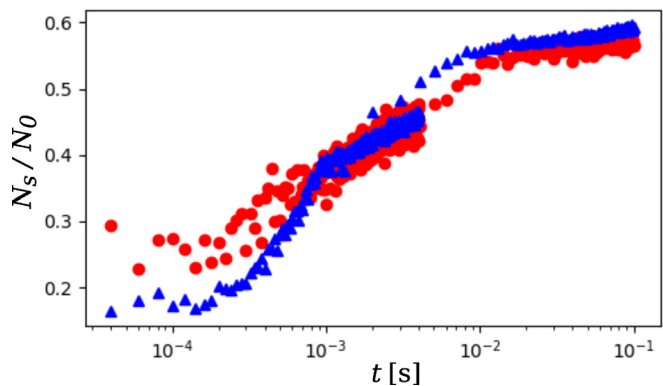


FIG. 3. Coaxial transfer efficiency N_s/N_0 from the master cell into cell A as a function of time t after the barrier is removed. Data are shown for $N_0 = 1.5 \times 10^8$ (red circles) and 5.2×10^8 (blue triangles), where fast transfer events correspond to times $t \leq 10^{-4}$ s.

Both datasets show a similar trend: The efficiency is approximately constant at short times (fast transfers, $N_s/N_0 \approx 0.2\text{--}0.3$ for $t \leq 10^{-4}$ s), then it grows, and becomes roughly constant again at long times (slow transfers, $N_s/N_0 \approx 0.5\text{--}0.6$ for $t \geq 10^{-2}$ s).

The transfer efficiency can be understood by using a simple model to describe the steady states. The density and potential are taken to be constant in each cell, with a discontinuity at the interface. Thus, the potential in each cell (M and A) is given by Eq. (1) where the lengths L and parameter $\eta \equiv 1 + 2 \ln r_w/r_p$ are constants for each cell, and the number of particles in each cell N_m and N_s are to be determined. For the fast (collisionless) steady state, we enforce conservation of particles $N_0 = N_m + N_s$, continuity of particle flux at the interface $N_m v_m/L_m = N_s v_s/L_s$, and parallel energy in each cell

$$\begin{aligned} m_e v_m^2 &= 2e(\phi_0 - \phi_m); \\ m_e v_s^2 &= 2e(\phi_0 - \phi_s - V_s), \end{aligned} \quad (3)$$

where v is the axial velocity of electrons in each cell, m_e is the electron mass, ϕ_0 is potential of the initial master cell plasma, and V_s represents a uniform bias applied to the electrodes of the storage cell. Combining these expressions gives a quadratic formula for the transfer efficiency

$$\left(1 + R_L^3 \frac{\eta_s}{\eta_m}\right) \left(\frac{N_s}{N_0}\right)^2 + \left(\frac{-4\pi\epsilon_0 V_s L_m R_L^2}{e \eta_m N_0} - R_L^2 - 2\right) \frac{N_s}{N_0} + 1 = 0, \quad (4)$$

where $R_L \equiv L_m/L_s$ is the ratio of plasma lengths in each cell, and the efficiency is given by the lesser root of Eq. (4) for which $0 < N_s/N_0 < 1$.

With the front plate serving as the boundary between the two cells, we estimate that $L_m = 0.23$ m and $L_s = 0.18$ m for $N_0 = 10^8$ and $r_p = 1$ mm, so $R_L = 1.28$. In this case, if $V_s = 0$ V, then $N_s/N_0 \approx 0.36$. The roots become imaginary for $V_s < -1.9$ V (for which $N_s/N_0 \approx 0.66$) since the model becomes invalid due to particle trapping. The efficiency can be increased by applying a small negative voltage V_s to the storage cell electrodes or decreased using a positive voltage (due to anti-shielding). It can also be increased by reducing R_L , for example, by using a shorter master cell plasma (e.g., only spanning electrodes M4 and M5). However, this also reduces N_0 and therefore may be detrimental to the goal of maximizing N_s .

In order to study anti-shielding in the storage cell, experiments were conducted where a uniform bias V_s was applied to electrodes A2–A5 during the transfer. Figure 4 shows the efficiency in the collisionless regime ($t = 100$ μ s) as a function of V_s , for a plasma with $N_0 = 10^8$ and $r_p = 1$ mm. As expected, a positive bias reduces the efficiency due to anti-shielding and vice versa for small negative bias, although larger negative voltages reduce the efficiency due to the trapping of electrons in the master cell. Although the model seems to capture the qualitative features of the experimental data, it fails to predict N_s/N_0 quantitatively, especially near $V_s = 0$. The disagreement is not surprising given the simplicity of Eq. (3). A more accurate description would likely need to account for the variation of L with ϕ and the finite extent of the interface region.

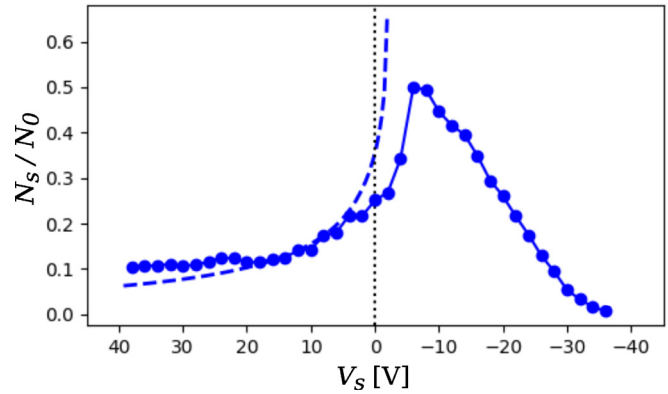


FIG. 4. Coaxial fast transfer efficiency N_s/N_0 as a function of bias V_s applied to the cell A electrodes. Here, $N_0 = 10^8$, $r_p = 1$ mm, and the data are compared to a simple model (dashed) which is described in the text.

On collisional timescales, the plasma shields the interface by adjusting its density to maintain equipotential along the field; thus, the efficiency (with $V_s = 0$) can be calculated in a similar way by enforcing $\phi_m = \phi_s$. This results in

$$\frac{N_s}{N_0} = \frac{1}{1 + R_L \eta_s / \eta_m} \approx 0.56. \quad (5)$$

This prediction is consistent with the data in Fig. 3. However, on collisional timescales, unity efficiency can be achieved by applying a sufficiently deep potential well (i.e., with $V_s > 0$). Thus, the collisionless regime is characterized by anti-shielding behavior, and the efficiency can be improved by biasing the electrodes negatively. In contrast, the collisional regime is characterized by regular shielding, and efficiency can be improved using a positive bias.

V. OFF-AXIS TRANSFER

The transfer of plasmas into the off-axis cells is complicated relative to the coaxial case described in Sec. IV due to the transverse $\mathbf{E} \times \mathbf{B}$ drift dynamics. In this case, the plasma is excited to a large-amplitude circular diocotron orbit using the autoresonant drive technique described in Sec. III, and the potential barrier separating the master and storage cells is lowered as the plasma azimuthally transits the storage cell location. The resulting dynamics have been investigated previously²⁸ and are summarized briefly here.

When the barrier is lowered (i.e., electrodes M5, FP, and S1 are grounded), the electrons transit both cells, bouncing between potential barriers at electrodes M1 and S6 just as in the coaxial case. However, since the plasma is located off the axis of the master cell (and possibly also that of the storage cell), the plasma induces image charges in the wall of each cell and undergoes transverse diocotron-like drift motion. Since the axial bounce motion is rapid (~ 1 MHz) relative to that of the diocotron orbits (1–10 kHz), the plasma behaves as a rigid column, and so, the dynamics can be described by averaging the image field over the bounce cycle.

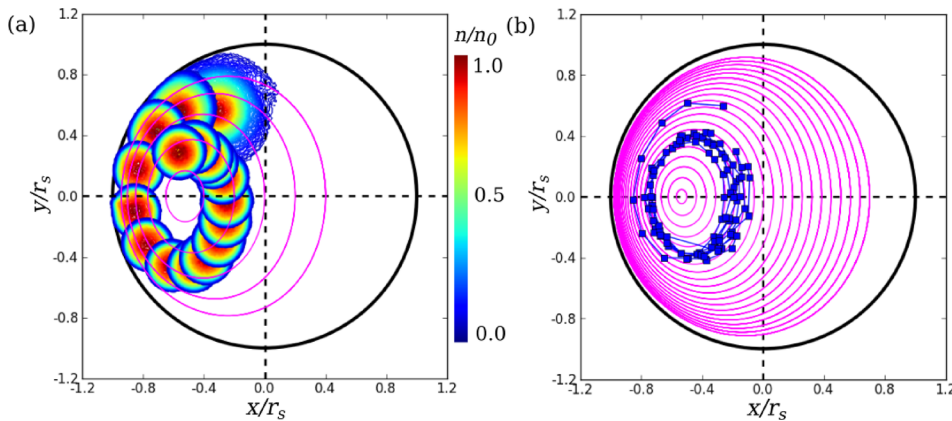


FIG. 5. Bounce-average diocotron orbit of a plasma spanning both the master cell and the off-axis storage cell C. (a) CCD images of the electron density in the storage cell frame over the first period ($t=0-800\ \mu\text{s}$). (b) Trajectory of the plasma density centroid over ~ 6 periods ($t=0-5\ \text{ms}$). The orbits proceed in the counter-clockwise direction, and data are compared to predictions of a simple model (magenta lines). See text for details. Adapted from Hurst et al.²⁸

An example of this behavior in cell C is shown in Fig. 5, including CCD images of the electron density and the trajectory of the plasma density centroid. Here, the storage cell orientation is chosen such that the master cell symmetry axis lies on the negative x -axis. Over the first half of the first orbit, the plasma experiences a transient phase where outer particles are lost to the wall and the radius decreases. After this, it settles into a stable, quasi-elliptical orbit within the bounds of the storage cell but offset from its axis. Figure 6 shows the particle number, plasma radius, and displacement in the storage cell frame over the course of six orbit periods, corresponding to the data in Fig. 5. In this case, the perpendicular drift dynamics occur on intermediate timescales (i.e., between the slow and fast regimes of the axial dynamics). The impact of the drift orbits on the axial transfer dynamics is not yet well understood and is left for future work.

Also shown in Fig. 5 are predictions for the orbit due to a simple model.²⁸ Here, the plasma is treated as a line charge ($r_p \rightarrow 0$) drifting under the influence of the bounce-average of the image field in the master and storage cells. Since the plasma explores only a small portion of the master cell (i.e., in r, θ) throughout an orbit, the master cell image field is taken to be a

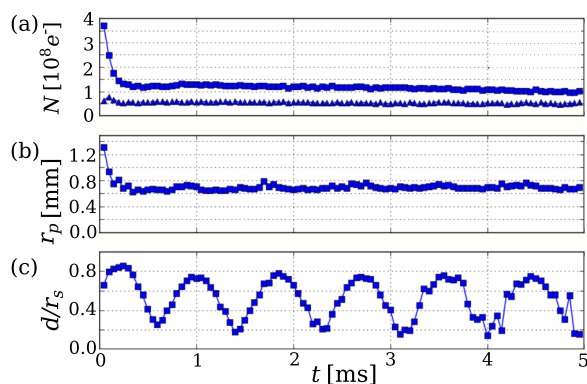


FIG. 6. Properties of a plasma during a bounce-average orbit in cell C, corresponding to the data in Fig. 5. (a) Total particle number N_0 (squares) and that in the storage cell N_s (triangles), (b) plasma radius, and (c) displacement from the storage cell axis.

constant. However, the plasma explores a fractionally larger range of positions in the storage cell, so the full nonlinear form of Eq. (2) must be considered.

These dynamics can be described by the Hamiltonian

$$H = -\alpha d \cos(\theta) + \ln(1 - d^2), \quad (6)$$

where α is a parameter describing the influence of the master cell relative to the storage cell, and the canonical coordinates are (p_θ, θ) , where $p_\theta = (\lambda B/2)d^2$ is the canonical angular momentum and $\lambda \equiv eN/L$ is the average line density.²⁹ Plasma trajectories are given by contours of constant H and are plotted in Fig. 5 as magenta lines. Following the initial transient (where the plasma experiences particle loss), the plasma orbit shape is in good agreement with Eq. (6) for $\alpha = 0.75$.²⁸ Unfortunately, α is difficult to calculate accurately due to finite-length corrections in the master cell¹⁹ and axial dynamics at the interface between the two cells, similar to that described in Sec. IV, so it is treated here as a fit parameter. If the line density in the two cells λ_m and λ_s are different (as the results in Sec. IV would suggest), then $\alpha \propto \lambda_m/\lambda_s$, and α may change over time due to axial relaxation (cf. Fig. 3) or particle loss.

The system described by Eq. (6) has a stable fixed point given by

$$(d^*, \theta^*) = \left(-\alpha^{-1} + \sqrt{\alpha^{-2} + 1}, \pi \right), \quad (7)$$

where the drift contributions from the master and storage cell exactly cancel. Previous work²⁸ showed that the plasma could be held stationary at this point by careful choice of the initial placement of the plasma, although it expanded quickly due to asymmetry transport.

The rapid particle loss observed in Fig. 5 is detrimental to the goals of multicell trap operation. However, if the plasma is positioned initially near the storage cell axis and the fast transfer scheme is used (cf. Fig. 3, $t < 100\ \mu\text{s}$), the bounce-average drift dynamics are unimportant. In this way, transfers can be conducted without the complication of perpendicular drift motion, although the efficiency is constrained due to the anti-shielding phenomenon discussed in Sec. IV. Figure 7 shows measurements of the transfer efficiency versus time during fast transfer into cells A (on-axis) and C (off-axis), where $N_0 = 2.5 \times 10^8$ and r_p

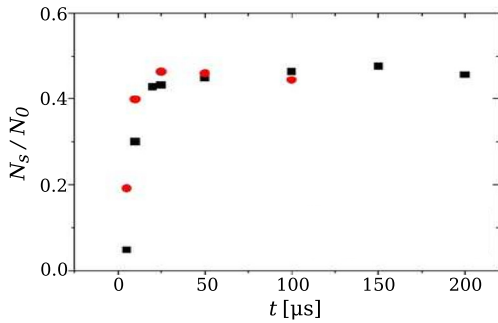


FIG. 7. Transfer efficiency over short timescales in the on-axis cell (A, red circles) and an off-axis cell (C, black squares). Similar equilibration time and collisionless steady states are observed in both cells.

~0.5 mm. The data are almost identical in the two cells, suggesting that the axial transfer dynamics at these short timescales is independent of the transverse location of the storage cell. Here, the master cell plasma is shortened by biasing electrodes M2 and M3 to voltage $V_c = -100$ V, so that $R_L \approx 0.83$, and the efficiency is increased relative to the data in Figs. 3 and 4. In this case, the simple model in Sec. IV predicts $N_s/N_0 = 0.49$, close to the value of ~0.45 observed in Fig. 7.

Discussed elsewhere³⁰ is a technique which has been used to conduct transfers into an off-axis cell on intermediate timescales. Here, the bounce-average orbits were damped toward the fixed point given by Eq. (7) using a feedback circuit connected to the segments of electrode B4. The plasma was held at this point and “squeezed” axially into the storage cell by negatively biasing the master cell electrodes. In this way, efficiency close to unity was achieved for transfer into an off-axis cell.

VI. STORAGE CELL CONFINEMENT

Once the plasma has been transferred into the storage cell (either on- or off-axis), the barrier separating the master and storage cells is raised to voltage $V_c = -100$ V, thus isolating the transferred plasma from that remaining in the master cell. At this point, the remaining master cell plasma can be returned to the axis by running the autoresonant chirp protocol in reverse.¹⁸ Here, it can

be combined with newly introduced particles, compressed using the RW, and eventually used for a subsequent transfer event. Thus, particle loss can be minimized, which is important for anti-matter applications. The plasma trapped in the storage cell can be compressed and confined using the RW and eventually extracted. In this section, we present studies of the radial transport and RW compression of plasmas trapped in the storage cells.

Plasma has been transferred individually into each of the four storage cells using the fast transfer technique, although plasmas have not yet been confined in multiple storage cells simultaneously. Shown in Fig. 8(a) is a combination of four images of plasmas confined in each of the storage cells; and their radial profiles are shown in panel (b). The off-axis trapped plasmas are spatially broader than the on-axis one due to expansion during the autoresonant drive (cf. Sec. III).¹⁸

Shown in Fig. 9 is the normalized particle number versus time for plasmas confined in each of the storage cells (without RW compression), where the initial plasma radii range from 0.5 to 0.8 mm and $N_0 \sim 8 \times 10^7$ (cells A and B) or 4×10^7 (cells C and D). For the cells with the largest radius (cells A and B), the plasma initially expands without particle loss. When the edge of the plasma reaches the wall (at $t \sim 10$ s), particle loss commences, and the plasma is completely gone within 100 s. The data for cells A and B are remarkably similar, indicating that radial transport is not dependent on the transverse location of the cell. In cells C and D, particle loss commences almost immediately following transfer into the cell, although the loss rate is much higher in cell D, likely due to the smaller wall radius.

Using the RW to counteract outward transport, plasmas have been held for >24 h in cells A and B, but roughly 20% of the particles were lost over this time. Plasmas were held in cell C for ~2 h, although this is likely not the limit. However, in cell D, the RW compression was not sufficient to counter the rapid outward expansion, and so, plasmas could not be held in cell D for longer than about 1 s. Plasma properties are shown versus time in Fig. 10 for RW experiments in cell C. Here, the RW is implemented directly following the plasma transfer, by applying phased sinusoidal voltages to the segments of electrode C4 at a frequency of 2 MHz and an amplitude of 800 mV. The particle loss observed during the first 5–10 s appears to be associated

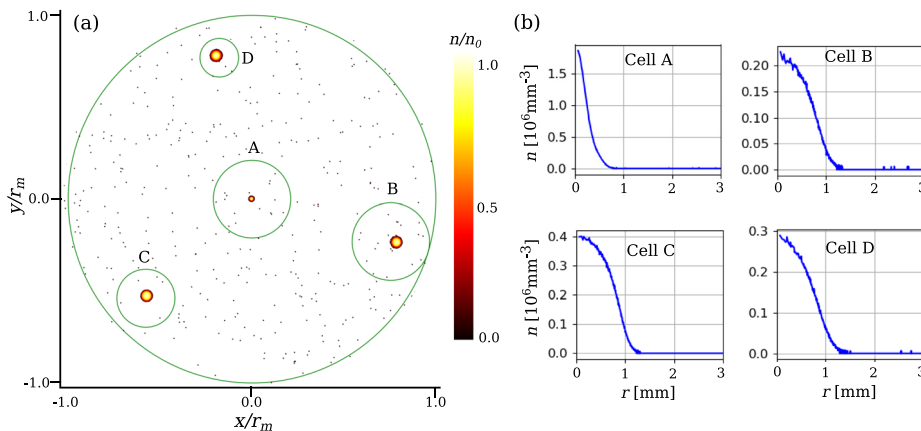


FIG. 8. Plasmas trapped in each of the four storage cells (not simultaneously), including (a) a combination of the four CCD images and (b) corresponding radial density profiles.

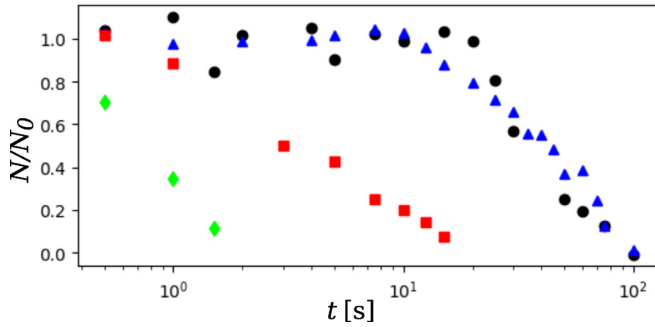


FIG. 9. Normalized particle number versus time (without RW compression) for the storage cells A (black circles), B (blue triangles), C (red squares), and D (green diamonds).

with poor RW compression of plasma at radii $\geq 0.3r_w$, possibly due to strong asymmetry-induced transport and/or higher-order terms of the RW field. However, the remaining particles reach a high-density steady state which persists as long as the RW is enabled. The particle loss shown in Fig. 10 can be avoided if the initial radial extent of the plasma is sufficiently small. However, this requires that expansion be kept at a minimum during the autoresonant drive and the transfer process.¹⁸ A second dataset is also shown where the RW is turned off at $t = 15$ s. Here, outward expansion is observed, although in this case the particle number is conserved since the plasma remains isolated from the wall throughout the time of observation.

In general, the free radial transport in the storage cells (i.e., without the RW) is characterized by the presence of a low-density tail, or “halo” in the density distribution, which has been observed previously in response to applied asymmetries.³¹ This is demonstrated in Fig. 11, which shows (a) the evolution of the radial density profile in cell A, and CCD images of the areal electron density distribution at (b) $t = 0$ s and (c) $t = 5$ s for a plasma with

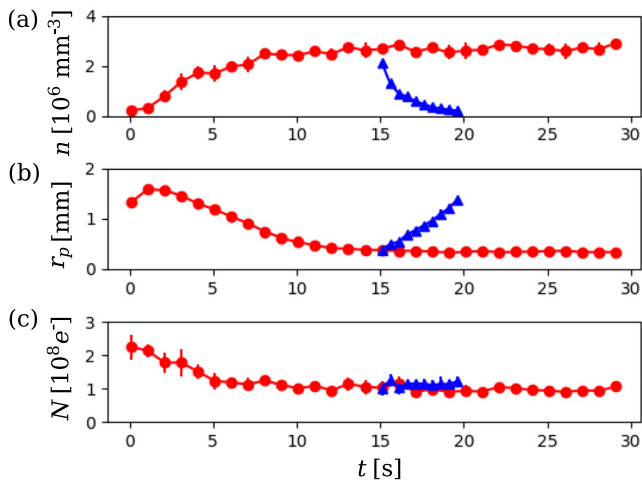


FIG. 10. Compression and confinement of a plasma in cell C using the RW (red circles): (a) the central density, (b) plasma radius, and (c) particle number. Also shown are data for which the RW is turned off at $t = 15$ s (blue triangles).

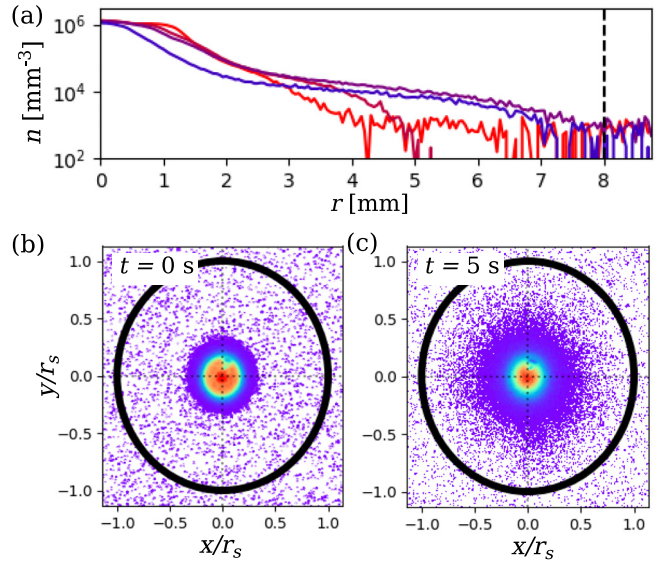


FIG. 11. Free relaxation of a plasma in cell A (on-axis), including (a) radial density profiles at $t = 0, 2, 5,$ and 20 s (red to blue), and CCD images of the electron density at (b) $t = 0$ and (c) $t = 5$ s. The low-density feature in the images near $x/r_s = y/r_s = 0.1$ is due to a defect in the phosphor screen.

$N = 10^9$. The halo forms and reaches the wall within ~ 5 s, after which the density profile decreases in an approximately self-similar way. These data imply that the radial transport increases substantially near the periphery of the cell relative to that near the center. Halo transport was observed ubiquitously in this prototype multicell device, as was the associated particle loss to the wall. It is thought to be associated with asymmetries due to structural twisting and kinking of the storage cell electrodes, likely related to the mechanical (compressional) design of the multicell structure which, in retrospect, lacked azimuthal rigidity.

VII. HIGH VOLTAGE CONFINEMENT

In Secs. II–VI, the confinement voltage of $V_c = -100$ V was used exclusively in order to study the physics of cell-to-cell transfer, bounce-average orbits, and plasma confinement in the storage cells. However, in order to confine large numbers of particles ($N \sim 10^{11}$ – 10^{12}), a practical multicell trap would need to operate with potentials on the order of kilovolts.¹⁵ To this end, a set of basic plasma confinement experiments were conducted in cell A with V_c ranging from -0.1 to -1 kV.

Plasmas were generated directly in cell A by biasing electrodes A1 and A6 to voltages V_1 and $V_6 = -100$ V as usual, but electrodes A2–A4 were biased to voltage $V_s > 0$ in order to create a deeper potential well. Once the desired particle number was reached (typically, filling the well so that $\phi \approx -V_s$), electrodes A1 and A6 were ramped up to voltage $V_c = -V_s$, and then, electrodes A2–A4 were ramped to ground. The plasma was then held in this state and diagnosed using the phosphor screen and CCD camera by grounding electrode A6.

Figure 12 shows the measured total particle number N as a function of time, for confinement voltages $V_c = -0.1, -0.25,$

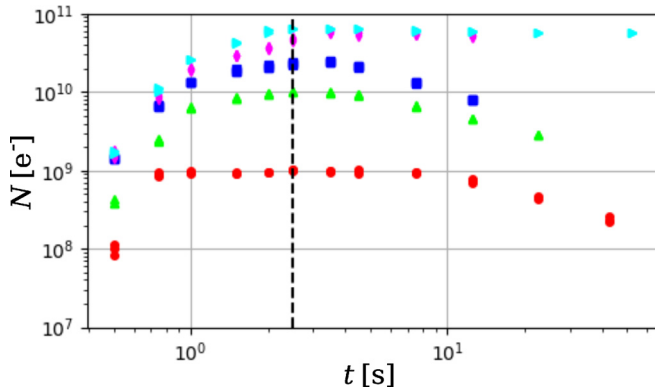


FIG. 12. Particle number versus time throughout the fill and confinement periods, for $V_c = -0.1$ (red circles), -0.25 (green triangles), -0.5 (blue squares), -0.75 (magenta diamonds), and -1 kV (cyan triangles). The fill was terminated at the vertical dashed line.

-0.5 , -0.75 , and -1 kV. Here, the well is filled over the course of 2.5 s, at which point (shown by the dashed vertical line) the plasma is isolated and the confinement is studied. For $V_c = -100$ V, $N \approx 10^9$ is achieved, and particles are eventually lost on a ~ 60 s timescale (in agreement with Fig. 9).

For $V_c = -1$ kV, N approaches 10^{11} . However, this result is misleading. The experiments with $V_c = -0.75$ and -1 kV show that N remains constant over time, rather than eventually

decaying like the other cases. This appears to be due to the formation of a steady-state discharge where electron losses are replenished by ionizing the background gas in the trapping region. This phenomenon is discussed in further detail below.

Figures 13(a)–13(d) show radial density profiles of the plasma throughout the filling and confinement periods, for $V_c = -0.5$ and -1 kV. During the fill process, the central density quickly reaches a maximum, at which point the profiles grow radially. For $V_c = -0.5$ kV, the profile evolution is similar to that in Fig. 11 for $V_c = -0.1$ kV. Here, the halo develops quickly and reaches the wall during the fill process; then, during confinement, the profile decays almost self-similarly. For $V_c = -1$ kV, the steady-state discharge is observed, beginning during the fill and persisting throughout the confinement period. Here, the plasma obtains a steady-state profile consisting of a high-density core, a low-density tail, and a sheath region close to the wall.

Figures 13(e)–13(h) show CCD images of the plasma density for $V_c = -0.5$ and -1 kV, both 2 s into the filling period and 2 s into the confinement period. In all cases, low-density non-axisymmetric structures can be seen in the region outside the plasma core, indicating the existence of non-diffusive, wave-like transport. Interestingly, these structures are observed in both the steady-state regime [$V_c = -1$ kV, panel (h)] and the decaying regime [$V_c = -0.5$ kV, panel (f)]. Alternatively, the data in Fig. 11 for $V_c = -0.1$ kV show an axisymmetric density distribution, consistent with diffusive radial transport.

We describe here a possible mechanism for the steady-state discharge phenomenon, although further data are needed

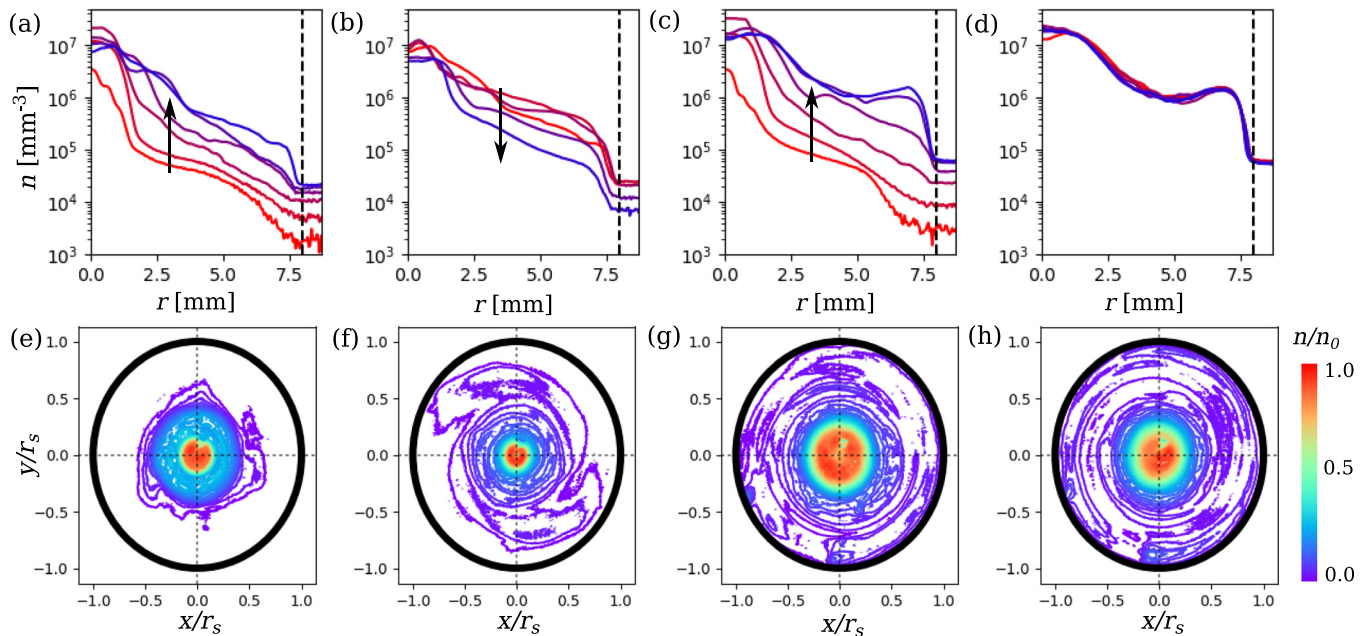


FIG. 13. Evolution of the average radial density profile with time (a)–(d) and snapshots of the density distribution (e)–(h) during the fill and hold periods with high-voltage confinement potentials, where the fill is terminated at $t = 2.5$ s. Panels (a), (b), (e), and (f) correspond to $V_c = -0.5$ kV for times (a) $t = 0.5, 0.75, 1.0, 1.5, 2.0,$ and 2.5 s; (b) 2.6, 3.5, 4.5, 7.5, and 12.5 s; (e) 2 s; and (f) 4.5 s. Panels (c), (d), (g), and (h) correspond to $V_c = -1$ kV for times (c) $t = 0.5, 0.75, 1.0, 1.5, 2.0,$ and 2.5 s; (d) 2.6, 3.5, 4.5, 7.5, 12.5, 22.5, and 52.5 s; (g) 2 s; and (h) 4.5 s. Time proceeds from red to blue in panels (a)–(d), as indicated by the arrows. Note the development of a steady-state discharge for $V_c = -1$ kV. The low-density feature at $(x/r_s, y/r_s) \approx (0.1, 0.1)$ is due to a defect in the phosphor screen.

to verify this description. Figure 13 demonstrates that there is a substantial outward flux of electrons toward the wall. This liberates electrostatic energy and results in heating of the plasma. In this way, the plasma can be heated to the point where collisions between plasma electrons and background neutrals can result in ionization, thus providing a source of electrons and a sink for thermal energy. The discharge is continuously driven by the power supply which holds the trap electrodes at constant potentials. The ions, which are born in a deep negative potential well, are presumably lost radially to the wall at a faster rate than the electrons due to the large gyroradius.

When the electron source dominates over losses to the wall, the potential well is eventually filled with electrons. At this point, electrons can also be lost axially through the applied potential barriers, and so, the source is balanced by both radial and axial losses. Axial losses have been detected as a current of ~ 5 nA to the phosphor screen. These steady-state discharges have been found to persist for at least an hour without any active control. Interestingly, the diocotron mode amplitude was observed to vary periodically at roughly 1 Hz, which may be indicative of various instabilities.

VIII. SUMMARY AND CONCLUSIONS

Presented here are the results of a comprehensive set of experiments with electron plasmas in a prototype multicell Penning-Malmberg trap, with the goal of long-term, high-capacity positron storage.^{12,14,15} The major objective of this project was to transfer plasmas from a large-diameter master cell into each of four small-diameter storage cells, both coaxial and non-coaxial, and to hold them in the storage cells using RW compression for hours or more. The goal is to do this with minimal particle losses (since antiparticles are difficult to produce) and with plasma space charge potentials ranging up to a kilovolt so as to maximize the storage capacity of the trap. Long-term objectives are to operate multiple storage cells simultaneously and to develop a robust multicell electrode design that can be scaled up to accommodate a greater number of storage cells. Some of these goals were realized, while others remain for future research and development.

Here, we have demonstrated successful transfer of plasma into each of the four storage cells. In some cases, long-term confinement in both on-axis and off-axis storage cells was achieved using RW compression. Interesting plasma behavior was observed and studied during each step of the multicell trap operation. However, plasmas in the prototype device were subject to rapid radial expansion and particle loss thought to be associated with electrical and mechanical asymmetries. Due in part to these problems, we were unable to achieve the goals of long-term confinement of plasma in the smallest storage cell ($r_w = 4$ mm) and good confinement in the largest storage cell ($r_w = 8$ mm) with space charge potential exceeding 0.5 kV. Simultaneous operation of multiple storage cells has not yet been attempted due to lack of necessary electrical equipment.

The axial dynamics of the plasmas were studied during transfer into the on-axis storage cell. Two regimes were identified: A fast regime ($t \lesssim 100 \mu\text{s}$) where the plasma reached a collisionless equilibrium between the master and storage cells and a

slow regime ($t \gtrsim 1$ ms) where the plasma equilibrated axially due to collisions. In the fast regime, the transfer efficiency was reduced due to anti-shielding phenomena. In the slow regime, unity efficiency is possible by creating a potential well in the storage cell.

Plasmas were displaced across the magnetic field to the location of the off-axis cells using autoresonant drive of the diocotron mode.^{18,21} However, under most conditions, they expanded significantly during this process, with negative implications for the subsequent transfer into and confinement in the storage cells. Transfer into the off-axis cells was further complicated by a novel type of hybrid diocotron orbit due to the axial bounce-average of the image field in the master and storage cells.²⁸ These orbits take place on intermediate drift timescales between that of the fast and slow axial transfer dynamics. However, other work shows that, through careful manipulation of these orbits, one can achieve transfer efficiency approaching unity.³⁰

In general, plasma confinement in the storage cells was relatively poor. It appears that mechanical asymmetries in the electrode structure led to the formation of a low-density “halo” which propagates radially away from the plasma core and eventually reaches the wall. The RW technique was capable of containing only particles near the storage cell axis; thus, in order to confine plasmas without particle loss, the plasma must have initially small dimensions ($r_p/r_w \ll 1$) and relatively weak radial transport.

In the largest storage cell (B) at low space charge, these conditions were largely met and plasma was confined for over a day with only minor losses. In the smallest storage cell (D), the transport was sufficiently rapid that the RW was not able to contain the plasma, which was lost to the wall within about 1 s. Additional confinement studies in the on-axis storage cell (A) showed that the transport rate increased as the space charge potential was raised above 100 V, thus heating the plasma. For potentials exceeding 500 V, a steady state discharge was observed, likely due to ionization of background neutrals. This could be avoided by improving the vacuum, which would require better pumping and better conductance through the electrode structure.

Our recommendations for future efforts in research and development of the multicell trap concept are the following: Most importantly, the radial transport must be minimized, both in the storage cells and during plasma manipulation. In order to accomplish this, the plasma must be kept in a region of uniform magnetic field,²⁴ it must be kept at a relatively low temperature (i.e., through cyclotron cooling),¹⁶ and the confinement region must be azimuthally symmetric to a high degree of accuracy.¹⁷ The prototype apparatus suffered from mechanical asymmetries due to the compressional nature of the design, which permitted the storage cells to deform slightly. Future efforts would benefit significantly from a more rigid design. Autoresonant displacement of the plasma should be accomplished quickly to avoid expansion. Expansion can be avoided somewhat by using short master cell plasmas, but then many subsequent transfer events are required to reach the storage cell capacity. Transfer into a cell with pre-existing plasma, sometimes called “stacking,”³² has

been attempted but not studied in detail. Preliminary experiments indicate that stacking tends to cause radial transport and halo formation.

High-efficiency transfer of plasma into off-axis cells can be conducted on slow or intermediate timescales, but care should be taken to avoid expansion during this process as well; otherwise, fast transfers with lower efficiency can be implemented without expansion. The storage cell wall radius should be sufficiently large compared to the plasma radius to prevent losses during the early stages of RW compression. One might also consider using higher-order (e.g., quadrupolar) RW fields in order to provide compression at larger radii. We anticipate that, by implementing some combination of these techniques, the radial transport could be reduced to the point where multiple-cell operation and long-term storage of plasmas with kilovolt potentials will be possible.

ACKNOWLEDGMENTS

We acknowledge expert technical assistance from the late Gene Jerzewski. This work was supported by the UCSD Foundation, the U. S. Defense Threat Reduction Agency, and the U. S. DOE, Grant No. DE-SC0019271.

REFERENCES

- ¹T. M. O'Neil, *Phys. Today* **52**(24), 24 (1999).
- ²D. H. E. Dubin and T. M. O'Neil, *Rev. Mod. Phys.* **71**(1), 87 (1999).
- ³J. R. Danielson, D. H. E. Dubin, R. G. Greaves, and C. M. Surko, *Rev. Mod. Phys.* **87**(1), 247 (2015).
- ⁴T. M. O'Neil, *Phys. Fluids* **23**(11), 2216 (1980).
- ⁵C. M. Surko and R. G. Greaves, *Phys. Plasmas* **11**(5), 2333 (2004).
- ⁶E. M. Hollmann, F. Anderegg, and C. F. Driscoll, *Phys. Plasmas* **7**(7), 2776 (2000).
- ⁷J. R. Danielson, C. M. Surko, and T. M. O'Neil, *Phys. Rev. Lett.* **99**, 135005 (2007).
- ⁸G. B. Andresen, M. D. Ashkezari, M. Baquero-Ruiz, W. Bertsche, P. D. Bowe, E. Butler, C. L. Cesar, S. Chapman, M. Charlton, A. Deller *et al.*, *Nature* **468**, 673 (2010).
- ⁹M. R. Natisin, J. R. Danielson, and C. M. Surko, *Appl. Phys. Lett.* **108**, 024102 (2016).
- ¹⁰D. B. Cassidy and A. P. Mills, *Nature* **449**, 195 (2007).
- ¹¹H. Saitoh, T. S. Pedersen, U. Hergenbahn, E. V. Stenson, N. Paschkowski, and C. Hugenschmidt, *J. Phys.: Conf. Ser.* **505**, 012045 (2014).
- ¹²J. R. Danielson, N. C. Hurst, and C. M. Surko, *AIP Conf. Proc.* **1521**, 101 (2013).
- ¹³D. W. Fitzakerley, M. C. George, E. A. Hessels, T. D. G. Skinner, C. H. Storry, M. Weel, G. Gabrielse, C. D. Hamley, N. Jones, and K. Marable, *J. Phys. B: At., Mol. Opt. Phys.* **49**, 064001 (2016).
- ¹⁴C. M. Surko and R. G. Greaves, *Radiat. Phys. Chem.* **68**, 419 (2003).
- ¹⁵J. R. Danielson, T. R. Weber, and C. M. Surko, *Phys. Plasmas* **13**, 123502 (2006).
- ¹⁶T. M. O'Neil, *Phys. Fluids* **23**(4), 725 (1980).
- ¹⁷J. M. Kriesel and C. F. Driscoll, *Phys. Rev. Lett.* **85**(12), 2510 (2000).
- ¹⁸C. J. Baker, J. R. Danielson, N. C. Hurst, and C. M. Surko, *Phys. Plasmas* **22**, 022302 (2015).
- ¹⁹N. C. Hurst, J. R. Danielson, C. J. Baker, and C. M. Surko, *AIP Conf. Proc.* **1668**, 020003 (2015).
- ²⁰T. Mohamed, H. Imao, N. Oshima, A. Mohri, and Y. Yamazaki, *Phys. Plasmas* **18**(3), 032507 (2011).
- ²¹J. Fajans, E. Gilson, and L. Friedland, *Phys. Rev. Lett.* **82**(22), 4444 (1999).
- ²²K. S. Fine and C. F. Driscoll, *Phys. Plasmas* **5**(3), 601 (1998).
- ²³B. P. Cluggish and C. F. Driscoll, *Phys. Rev. Lett.* **74**(21), 4213 (1995).
- ²⁴D. Eggleston, K. J. McMurtry, A. A. Kabantsev, and C. F. Driscoll, *Phys. Plasmas* **13**, 032303 (2006).
- ²⁵N. C. Hurst, J. R. Danielson, D. H. E. Dubin, and C. M. Surko, *Phys. Rev. Lett.* **117**, 235001 (2016).
- ²⁶J. D. Moody and J. H. Malmberg, *Phys. Rev. Lett.* **69**(25), 3639 (1992).
- ²⁷C. Hansen and J. Fajans, *Phys. Rev. Lett.* **74**(21), 4209 (1995).
- ²⁸N. C. Hurst, J. R. Danielson, C. J. Baker, and C. M. Surko, *Phys. Rev. Lett.* **113**, 025004 (2014).
- ²⁹J. Notte, J. Fajans, R. Chu, and J. S. Wurtele, *Phys. Rev. Lett.* **70**(25), 3900 (1993).
- ³⁰J. R. Danielson, N. C. Hurst, C. J. Baker, and C. M. Surko (in preparation).
- ³¹A. Kabantsev, C. Y. Chim, T. M. O'Neil, and C. F. Driscoll, *Phys. Rev. Lett.* **112**, 115003 (2014).
- ³²M. Ahmadi *et al.*, *Nat. Commun.* **8**, 681 (2017).